DFT and molecular docking study of the effect of a green solvent (water and DMSO) on the structure, MEP, and FMOs of the 1-ethylpiperazine-1,4-diium bis(hydrogenoxalate) compound

M. Medimagh, C.B. Mleh, N. Issaoui, A. S. Kazachenko, T. Roisnel, O.M. Al-Dossary, H. Marouani, L.G. Bousiakoug

DFT and Molecular Docking Study of the Effect of a Green Solvent (water and DMSO) on the Structure, MEP, and FMOs of the 1-Ethylpiperazine-1,4-diium bis(hydrogenoxalate) Compound

Mouna MEDIMAGH[a], Cherifa Ben Mleh[b], Noureddine ISSAOUI[a*], Aleksandr S. Kazachenko[c,d,e], Thierry Roisnel[f], Omar M. Al-DOSSARY[g], Houda MAROUANI[b], Leda G. Bousiakoug[h]

[a]*University of Monastir, Laboratory of Quantum and Statistical Physics (LR18ES18), Faculty of Sciences, Monastir 5079, Tunisia.*
[b]*University of Carthage, Laboratory of Chemistry of Materials (LR13ES08), Faculty of Sciences of Bizerte, 7021, Tunisia.*

[c] *Siberian Federal University, pr. Svobodny, 79, Krasnoyarsk, 660041, Russia*

[d]*Institute of Chemistry and Chemical Technology, Krasnoyarsk Science Center, Siberian Branch, Russian Academy of Sciences, Akademgorodok, 50/24, Krasnoyarsk, 660036 Russia*

[e] *Prof. V.F. Voino-Yasenetsky Krasnoyarsk State Medical University of the Ministry of Healthcare of the Russian Federation, st. Partizan Zheleznyak, bld. 1, Krasnoyarsk, 660022, Russia*
[f]*Centre de Diffractométrie X, UMR 6226 CNRS, Unité Sciences Chimiques de Rennes, Université de Rennes I, 263 Avenue du Général Leclerc, Rennes, 35042, France*

[g]*Department of Physics and Astronomy, College of Science, King Saud University, PO Box 2455, Riyadh 11451, Saudi Arabia.*

[h]*IMD Laboratories Co, R&D Section, Lefkippos Technology Park, NCSR Demokritos PO Box 60037, 15130 Athens, Greece*

* Corresponding authors: Noureddine ISSAOUI, email: issaoui_noureddine@yahoo.fr

Abstract—We report in this study the influence of green solvents (water and DMSO) effect in structural parameters, frontier molecular orbital's (FMO's) and molecular electrostatic potential surface analysis (MEPS) of 1-ethylpipérazine-1,4-diium bis (hydrogenoxalate) (1EPBH) compound by means of DFT method. The compound has been examined by signal-crystal X-ray diffraction (XRD), infrared (IR) and nuclear magnetic resonance (NMR) spectroscopy. The theoretical calculations were carried out by density functional theory (DFT) method by using B3LYP/6-311++G(d,p) as the basis set. The Atom Centered Density Matrix propagation (ADMP) dynamic approach has been used. Based on the density functional theory calculation, a series of studies have been carried out to determine the noncovalent interactions in the 1EPBH compound. The types and strengths of interactions between hydrogen bonds have been established using the atoms in molecule method (AIM), electron localization function (ELF) and localization orbital locator (LOL). The average local ionization energy (ALIE) study has

been carried out. The Hirsfeld surface analysis has been employed to examine the nature of intermolecular contacts in the crystal structure. The strong and weak attractive, repulsive, and van der Waals interactions in the 1EPBH molecule have been determined by the reduced density gradient method (RDG). The natural bonding orbital (NBO) and the Mulliken charges have been computed for the investigated molecule with the density functional theory. The ^{13}C and ^{1}H nuclear magnetic resonance has been applied to confirm the molecular structure. Fourier-transform (IR) and ultraviolet-visible spectra (UV-visible) of the 1EPBH compound has been recorded in the ranges of 4000–500 cm^{-1} and 250–400 nm, respectively. Finally, the biological activities of 1-Ethylpiperazine-1,4-diium bis(hydrogenoxalate) have been examined. It is shown that the investigated compound (chosen as a ligand) can serve as an important epilepsy and cancer inhibitor.

Keywords*:* DFT, ALIE, AIM, ELF, LOL, docking calculation.

1. Introduction

Study of heterocyclic compounds is of great importance for pharmaceuticals to discover antibiotics for the treatment of several infections [1]. Piperazine compounds is currently the very important building block used in medical drug discovery. A bibliography review founded that the piperazine derivatives are employed in many bioactive structures used in various therapeutic areas [2-4], e.g., as antifungal [5], antibacterial, antimalarial, and antipsychotic agents [6]. In particular, N-Ethyl piperazine combined with other groups can be used in the synthesis of enrofloxacin, which is an antibiotic used to treat bacterial infections, as well as other pharmaceutical compounds [7]. 1-Ethylpiperazine-1,4-diium bis (hydrogenoxalate) (1EPBH) can be used in drugs for treating epilepsy and cancer diseases. This work reports on the X-ray diffraction (XRD) and theoretical characterization of a new 1EPBH hybrid molecule. We study the structural and physicochemical properties of the 1EPBH compound using the molecular modeling. The quantum mechanical simulations of the studied compound 1EPBH were determined with the DFT method. Hybrid density functional theory is employed for all theoretical calculations. This famous method gives a good precision of results. In our study, the optimized 1EPBH geometry is examined by the density functional theory (DFT) in the B3LYP/6-311++G(d, p) basis set. This level of theory is a high-power tool for optimizing the geometry and reproducing the experimental data of our compound 1EPBH. The computed geometrical parameters, molecular electrostatic potential (MEP) reactive sites, and frontier

molecular orbitals (FMOs) of the 1EPBH molecule in the gas and solvent (water and DMSO) phase are examined. To gain a deeper insight into the geometric stability of the investigated molecule, the DFT-based atom centered density matrix propagation is used. To provide the understanding of different types of interactions existed within our studied molecule, topological approaches were carried out. The noncovalent interactions in the 1EPBH molecule is exploited by the atoms in molecule (AIM), electron localization function (ELF), localization orbital locator (LOL), and average local ionization energy (ALIE) methods. The Hirshfeld surface analysis (HAS) is used to gain a more appropriate idea about the interactions of the compound with the neighboring molecules. The chemical bonding and visualization of weak interactions in the molecule under study are applied to investigate the reduced electron density gradient (RDG). The natural bonding orbital (NBO) analysis helped us to elucidate the inter- and intra-molecular charge transfer in the forming complex. The experimental data are obtained and justified by the vibrational analysis. In addition, the UV-visible absorption spectra was computed in the present work. The nuclear magnetic resonance (NMR) spectra of carbon ^{13}C and hydrogen ^{1}H in 1EPBH have been recorded and analyzed. Finally, to investigate the biological activity of the 1EPBH compound, the interaction of the ligand–receptor complexes are studied using the high-efficiency molecular docking calculation, which characterized our compound as a potential epilepsy and cancer inhibitor.

2. Experimental and theoretical details

2.1. Experimental and Synthesis details

The intensity measurements were performed on a Bruker D8 VENTURE AXS diffractometer [8] in MoK$\bar{\alpha}$ monochromatic radiation (λ = 0.71073 Å) at 150 K. The total number of measured reflections was 17058 (27.5° < θ < 2.7°); 2910 of them were independent and 2513 had the intensity $I > 2\sigma(I)$. The structure was solved directly using the SHELXL-97 program [9] and refined by the F^2-based full-matrix least-squares methods included in the WinGX software [10]. The molecular structure was visualized in the Diamond and Ortep system program [11, 12]. The crystallographic data are summarized in **Table 1**. The crystallographic information (CIF) on the structure under study was deposited in the Cambridge Crystallographic Data Centre as supplementary materials N° CCDC 2207825 and can be obtained for free via www.ccdc.cam.ac.uk/data_request/cif. The IR spectrum of 1EPBH is recorded in the region 4000-400 cm^{-1}. It was synthesized in the laboratory of chemistry of Matreials (LR13ES08) of Bizerte using Pellets containing the sample in question and KBr as a dispersant with 1.0 cm^{-1} resolution on a PERKIN ELMER FTIR Spectrophotometer.

An aqueous solution of $H_2C_2O_4$ (2 mmol in 10 mL water) was added to an aqueous solution of 1-ethylpiperazine (1 mmol in 10 ml of water). The obtained solution was stirred at 338 K for 1h and then left to stand at room temperature. Colorless single crystals of the title compound were obtained after some days. Schematically the reaction can be written:

$$C_6H_{14}N_2 + 2\,(H_2C_2O_4) \xrightarrow{338\,K} (C_6H_{16}N_2)(HC_2O_4)_2$$

2.2. Computational Details

In this study, all the calculations were performed in the Gaussian 09 software package [13] and the results were visualized through GaussView [14]. The geometric parameters of the 1EPBH compound in the gas and solvent (water and DMSO) phase were optimized by the DFT/B3LYP functional coupled with the 6-311++G(d, p) basis set. The molecular dynamic simulation was performed using the ADMP approach implemented in the Gaussian 09 software at the same level of theory. The MEP mapping and the FMO analysis were carried out using the IEFPCM solvation model. The density of states (DOS) in the gas, water, and DMSO phases was plotted using the Gauss-sum package [15]. The AIM, ELF, LOL, and ALIE topology data were calculated in the Multiwfn 3.8 [16] and AIMAll program [17]. The Hirshfeld surface study was carried out to elucidate the nature of interactions and their quantitative contributions to the crystal packing using the Crystal Explorer package [18]. The RDG method was exploited to analyze the interactions between hydrogen bonds using the Multiwfn and VMD visualization program [19]. The NBO and Mullikan charges were calculated at the same level of theory. In addition, the vibrational assignments of all bands of the investigated compound were determined. The UV-Visible spectrum of 1EPBH between 200 and 400 nm was recorded and analyzed. To establish the 3D crystal structure of the receptor in the docking assessment, the RCSB protein data bank was used [20]. The molecular docking simulation of the 1EPBH molecule was carried out in the MOE.2015 software [21].

2.3. Description of the Structure

The 1EPBH compound crystallizes in a monoclinic system (sp. gr. C2/c) with network parameters of a = 15.6403(14) Å, b = 5.6682(6), c = 29.901(3) Å, β = 103.649(3) Å, V = 2575.9(4) $Å^3$, and Z = 8. The unit cell of the $(C_6H_{16}N_2)(HC_2O_4)_2$ compound contains eight asymmetric units whose stacking along the three directions yields a 2D structure rich in hydrogen bonds (**Figure S1**). The ORTEP representation of the asymmetric unit of the structure under study is shown in **Figure S2**. It highlights the $(C_6H_{16}N_2)^{2+}$ organic cation and two $(HC_2O_4)^-$ hydrogenoxalate anions. The 1EPBH structure represents a cationic and anionic network. The cohesion of the crystal is ensured by hydrogen bonds. **Figure S3** presents the

projection of the structure along the [010] direction. It can be seen that hydrogenoxalate anions are linked through hydrogen bonds between which organic cations are intercalated with the formation of a 2D network. Similarly, in **Figure S3**, hydrogenoxalate anions are parallel to the (*b,c)* plane at x = 1/4 and 3/4 between which organic cations are localized in the (*b,c)* plane at x = 0 and 1/2. In addition, the crystal structure of the investigated compound is a 2D network of medium and weak O–H…O, N–H…O, and C–H…O hydrogen bonds distributed as shown in **Figure 1**. The distances between hydrogen bonds and their angles are summarized in **Table 2**. We note two bonds of the O–H…O type connecting the hydrogenoxalate groups with an average distance of 2.527 Å. Three bifurcated bonds of the N–H…O type link hydrogen atoms of the organic groups to oxygen atoms of the hydrogenoxalate groups $(HC_2O_4)^-$. The $d_{N...O}$ distances range from 2.754 Å and 3.244 Å. According to the Brown's criterion, these bonds are considered to be weak ($d_{N...O}$ < 2.73 Å) [22]. Six bonds of the C–H…O type link hydrogen atoms of the organic cation to oxygen atoms of the hydrogenoxalate groups with an average distance of 3.277 Å.

3. Results and Discussion

3.1. Optimized $(C_6H_{16}N_2)(HC_2O_4)_2$ Geometry

The molecular geometry of the $(C_6H_{16}N_2)(HC_2O_4)_2$ compound was optimized at the DFT/B3LYP level of theory in the 6-311++G(d, p) basis set for the gas phase and using the IEFPCM method for the solvent (water and DMSO) phase. The optimized molecular structure was found to have the C1 point group symmetry with ground state energy of –1103.59 a.u for the gas, –1103.64 a.u for water, and DMSO with a dipole moment of 2.70, 7.71, and 7.82 Debye, respectively. It should be noted that the solvent (water and DMSO) affects strongly the dipole moment μ of the investigated molecule, but does not affect the total energy. Further, the value of dipole moment of the DMSO is small compared than water. This is explains that the DMSO is capable for accepting hydrogen bonds. The selected parameters (bond lengths and angles) and their graphical forms are given in **Table S1** and shown in **Figure 2**. The data of the theoretical calculation were compared with the experimental parameters. It can be seen in **Table S1** that, according to the DFT and XRD data, the C–H bond lengths between atoms in the 1EPBH molecule for the gas and solvent effect were (1.089, 1.095) A° and (0.980, 0.991) A°, respectively. All C–C bond lengths ranged between 1.524–1.549 A° (B3LYP) and 1.516–1.560 A° (XRD). In addition, the N_7–H_8, N_7–H_9, and N_{16}–H_{17} bond lengths in piperazine are 1.016–1.644 A° (theory) for the gas phase and 1.020–1.074 A° for the solvent. Eight C–O bond lengths in the oxalate lie between 1.196–1.360 A° in the theory and 1.209–1.313 A° in the

experiment for both the gas and solvent. Further, according to the data given in **Table S1**, the O25–H17 interatomic spacing corresponds to the overall highest bond length like 1.419 A°, 1.616 A°, and 1.612 A° for the gas, water, and DMSO solvent and the O37–H8 spacing is 1.028 A° for the gas, 1.577A° for water, and 1.572 A° for DMSO. These largest bond lengths are indicative of the weak interaction between oxygen and hydrogen atoms due to the effect of the solvent. The corresponding calculated maximum bond angle was between N_{16}–H_{17}–O_{25} (170.9°) for the gas and between N_7–H_8–O_{37} (□168°) for the solvent phase. The minimum bond angle was between H_{22}–C_{21}–H_{23} for the gas (107.1°), water (108.4°), and DMSO (108.3°). The DFT calculation yielded the moderate hydrogen angles between H_8–O_{37}–C_{36} (118.3° and □130° for the gas and solvent phase), H_{17}–O_{25}–C_{26} (117.9° for the gas and □121° for water and DMSO), N_{16}–H_{17}–O_{25} (170.9° for the gas), and N_7–H_8–O_{37} (163.40°, 168.2°, and 168.9° for the gas, water, and DMSO, respectively). These hydrogen bond parameters stabilize the molecular structure of the compound under study. In addition, we note that the calculated parameters are very similar to the experimental data. Thus, the results obtained shows that the solvent (water and DMSO) increases the O–H bond length and decreases the N–H bond length and almost no changes in the C–C and C–H bonds in the 1EPBH molecule were found.

3.2. The ADMP Molecular Dynamics Simulation of the 1EPBH Compound

The Ab initio molecular dynamics (MD) calculations exploited an extended Lagrangian MD method, which contains atom-centered Gaussian basis functions and one particule electronic density matrix propagation [23, 24]. This method is known as atom centered density matrix propagation (ADMP) [25, 26]. In this work, the stability of the DFT/B3LYP/6-311++G(d, p) optimized geometries was evaluated using the ADMP molecular dynamic approach at 300 K. **Figure 3** shows the plots of total Hartree energy Δ*E* versus trajectory time (fs) for the 1EPBH gas, water, and DMSO solvent obtained by the ADMP method. The entire ADMP trajectory for the investigated compound in different phases was built in a total period of time of 30 fs. As can be seen in **Figure 3**, the ADMP method disclosed the high stability of the 1EPBH molecule with negligible changes in the total energy. It is clearly seen that the optimized structure (t = 0 fs) for different phases (gas, water, and DMSO) is consistent with the global minimum in the total energy curve. In addition, we note that the superposition of the water and DMSO curves shows that the solvent does not affect the total energy. Thus, the ADMP molecular dynamic calculation proved that the geometries optimized using the DFT calculation match efficiently to the global minima.

3.3. MEP Surface Analysis

To understand the relative polarity of the investigated compound, we used the MEP surface analysis, which is a very helpful descriptor for studying the sites of electrophilic (electron deficiency) and nucleophilic (electron excess) reactions and hydrogen bonding interactions [27]. In general, the MEP surface analysis reveals charge distributions in molecules. In this study, the MEP was generated for the 1EPBH gas and solvent (water and DMSO) effect using the Gaussian program at the same level of theory (B3LYP/6-311++G(d, p)); the plot is presented in **Figure S4**. In the MEP picture of the investigated compound, the potential is shown by different colors: the most negative regions are colored in red (strong repulsion), the most positive regions are blue (strong attraction), and the zero potential regions are green. In this figure, the electrostatic potential surfaces are plotted between –5.690 e-2 and 5.690 e-2. Importantly, the highest potential is observed at a level of oxygen atoms of the oxalate group; on the other hand, the most positive potential is observed at a level of hydrogen atoms. This facilitates the formation of hydrogen bonds between anions and cations.

3.4. FMO (HOMO–LUMO) Analysis

The frontier molecular orbitals (HOMO–LUMO) are widely used by physicists and chemists to study the chemical reactivity and the electrical and linear- and nonlinear optical proprieties of molecules [28]. The quantum calculation of 1EPBH was carried out by the DFT method at the 6-311++G(d, p) level using the GaussView 09 software. The HOMO–LUMO 3D pictures of the 1EPBH in the gas phase and solvent (water and DMSO) are presented in **Figure S5**. The red and green color in the figure correspond to the positive and negative sites of the molecule. It can be clearly seen that the HOMO is localized over the entire molecule and the LUMO, over the oxalate group. The global chemical descriptors and energy band gap calculated for different phases are given in **Table 3**. The band gap energy is a critical parameter for determining the stability of the molecule. According to the closed shell principle (the main closed shell), the molecule is stable when the energy difference ΔE is large. Put this otherwise, the occupied molecular orbitals are the bonding and antibonding orbitals and the vacant orbitals are the antibonding ones. The respective HOMO and LUMO energies of the 1EPBH compound are –6.77 eV and –1.98 eV for the 1EPBH gas, –7.18 eV and –1.50 eV for water, and –7.18 eV and –1.49 eV for DMSO. The frontier orbital energy gap in the compound under study is very broad: ΔE = 4.79 eV for the gas and almost the same value for the solvent (5.68 for water and 5.69 eV for DMSO), which is greater than 3 eV [29]. These values do not allow electrons to pass from the valence to conduction band. The HOMO–LUMO gap suggests the high kinetic and thermodynamic stability [30]. In addition, the data given in the table show that the chemical

potential μ of the 1EPBH molecule is negative. It means that this compound is stable and does not decompose spontaneously into elements. The electronegativity χ of the 1EPBH molecule is 4.78 eV for the gas, 4.34 eV for water, and 4.33 eV for DMSO. This is higher than 1.7 eV; i.e., the 1EPBH molecule has a high electronegativity number and will attract electrons. Thus, 1EPBH is the best electron acceptor.

The DOS was obtained in the GaussSum 2.2 program to calculate the group contributions to the HOMO–LUMO orbitals (see **Figure S6**). The green and blue lines in the DOS spectrum correspond to the HOMO and LUMO levels [31]. The graphical DOS shows that the energy gap of the investigated compound is 4.79 eV for the gas, 5.68 eV for water, and 5.67 eV for DMSO. The results are approximated to both the energy gap $|\Delta E_{HOMO–LUMO}|$ and $|\Delta E_{DOS}|$ energy. Thus, we can conclude that the green solvent increases the HOMO–LUMO energy gap.

3.5. QTAIM Analysis

The quantum theory of atoms in molecule (QTAIM) is used to investigate physical, chemical, and biological processes [32, 33]. It elucidates the nature of the intra- and intermolecular hydrogen bonding on the basis of topological parameters at bond critical points (BCPs). In this study, we calculated the proprieties of each hydrogen bond at its BCPs using the AIMAll program (see **Figure 4** and **Table 4**). The hydrogen bonding strength increases with the electron density. Total electron density H_{BCP} with electron kinetic energy density G_{BCP} and electron potential energy density V_{BCP} at BCPs allows one to establish the nature of hydrogen bonding and strength of interactions between hydrogen bonds. Roza et al. [34] classified the hydrogen bond interaction as weak at $\nabla^2\rho(r) > 0$ and $H_{BCP} > 0$ (electrostatic), medium at $\nabla^2\rho(r) > 0$ and $H_{BCP} < 0$ (partially covalent), and strong at $\nabla^2\rho(r) < 0$ and $H_{BCP} < 0$ covalent). The molecular graph shows three types of hydrogen bonds: C–H...O, N–H...O, and O–H...N. All these interactions between proton and acceptor atoms satisfy all the criteria of the hydrogen bond interaction. According to the data given in **Table 4**, all the $\nabla^2\rho(r)$ and H_{BCP} values are positive, except for the case of two hydrogen bonds N_{16}–H_{17}...O_{25} and O_{37}–H_8...N_7. Hence, according to the criteria proposed by Roza et al**.**, all the hydrogen bonds are weak and electrostatic, except for the N_{16}–H_{17}...O_{25} and O_{37}–H_8...N_7 interactions, which are medium and partially covalent. Furthermore, the interaction energies $E_{interactions} < 12.0$ kcal/mol (for weak) and $12.0 < E_{interactions} < 24.0$ kcal/mol (for medium) [35]) indicate that two types of hydrogen bonds form between the organic and inorganic groups.

3.6. The ELF and LOL Analysis

In this study, the ELF and LOL were analyzed to understand and interpret the calculated electronic structure [36]. The topological parameters (ELF and LOL) were plotted in the Multiwfn software (**Figure 5**). The ELF and LOL color maps confirmed the occurrence of bonding and nonbonding electrons. The ELF map in **Figure 5** is determined in the range of 0.0–1.0 and colored in blue to red. The LOL map in **Figure 5b** ranges within 0.0–0.8. The high ELF and LOL values (red color around hydrogen atoms H2, H22, and H31) are indicative of the high localization of electrons. The blue region around carbon atoms is a delocalized electron cloud. The blue circle around nitrogen and the same oxygen atoms show the electron depletion region between the inner and valence layer. We noted also the white color at the centre of hydrogen atoms in the LOL map. This region indicates that the electron density exceeds the upper limit of the color scale (0.8).

3.7. The ALIE Study

The ALIE study provides information about the local reactivity of a molecule [37]. To calculate properly the ALIE of the 1EPBH compound, the electron must first be extracted from the point of system. The ALIE presentation in **Figure S7** shows that the electrostatic potentials of the molecule under study ranges between 0.00 and 27.92 Bohr units with charges between 0.00 and 2.00. The sigma bond, as well as the stable bond between atoms in the 1EPBH compound, are colored in blue (with a scale range from 0.00 to 0.500), which is enchanting protons [38]. It can be seen that the blue color corresponds to hydrogen atoms. The red region (with a scale range from 1.800 to 2.00) shows that the strongly localized electrons occur in core electrons in heavy atoms are carbon and oxygen in the 1EPBH molecule. This region presents also multiple bonds [39].

3.8. Intermolecular interactions analysis by the Hirshfeld surface

The analysis of intermolecular interactions using the Hirshfeld surface allows chemists to establish the behavior of intermolecular interactions in a crystal. The d_{norm} representation of the Hirshfeld surface was calculated using the Crystal Explorer 3.1 software for the oxalate groups and the organic cation independently. The intermolecular contacts were analyzed around each part of the asymmetric unit. The Hirshfeld surface shown in **Figure S8** was built using d_{norm} as a representation mode to generate the Hirshfeld surfaces of the organic cations, anion, and asymmetric unit in the $(C_6H_{16}N_2)(HC_2O_4)_2$ structure. The interactions between the organic cation and anion within the crystal are illustrated by the color gradient. This gradient varies from blue to red through white. This reflects the existence of the N–H....O and C–H...O

interactions. Further, the analysis of 2D fingerprints of the Hirshfeld surfaces of the molecular structure of the $(C_6H_{16}N_2)(HC_2O_4)_2$ compound revealed the atoms involved in close contacts and associated the numerical values with the previously-described surfaces. **Figure 6** shows a 2D footprint plot of all the contacts contributing to the Hirshfeld surface of the 1EPBH compound. The observed color is associated with the density of points occupying a specific region of the plot. These points are colored in blue and the light-gray points do not contribute to the analysis. The fraction of the O...H/H...O contacts is 63.5% of the total Hirshfeld surface; they consist of two narrow symmetric tips with $d_e + d_i \sim 1.8$ Å (label 1) suggesting the presence of C–H...O and N–H...O hydrogen bonds. The 2D plot has two weak peaks around $d_e + d_i \sim 2.6$ Å (label 2), which reveal the presence of close H...H contacts within the investigated compound. The fraction of the H...H contacts is 31.9% of all the interatomic contacts. The C...H/H...C contacts are related to a low participation (1.4%) of the Hirshfeld surface. The percentage of the contacts found in the crystal structure under study is shown additionally in **Figure 6**. Thus, the nature of interatomic interactions in this compound can be easily understood using the HSA and 2D plot. The electrostatic potential of the 1EPBH molecule was analyzed and determined using the CrystalExplorer 3.1 software with the CIF file (**Figure S9**). The electrostatic potential surfaces are plotted between –0.263 (red) and 0.332 (blue). The negative potential regions are assigned to oxalate anions, while the positive potential regions, to the organic cation (specifically, hydrogen atoms) is located on the organic cation. These results suggest the existence of the overall electrostatic attraction between the oxalate anions and organic cation.

3.9. The RDG Analysis

The RDG is an approach that allows one to analyze the noncovalent interactions in the investigated molecular system and to predict different weak interactions, e.g., the Van Der Waals and hydrogen bonding interactions and the steric effect [40, 41]. The RDG plots were calculated using the Multiwfn 3.8 and VMD 1.9.2 software (**Figure 7**). Within our molecule in **Figure 7a**, one can see three colors: green, red and blue, which correspond to the van der Waals, steric effect (repulsive) and H-bond interactions, respectively. The repulsive interaction (red region) is observed inside atoms of the organic units, which show a strong steric effect. In **Figure 7a**, this region has a positive sign $(\lambda 2)\rho$ between 0.01 and 0.05 a.u. The Van Der Waals interactions (the green region) can be seen between hydrogen atoms of the organic group. Another Van Der Waals interaction is observed between the inorganic and organic groups of the compound under study. The van der Waals interactions occur in the sign area of $(\lambda 2)\rho = 0$ (**Figure 7b**). In addition, dark blue spots in **Figure 7a** between the hydrogen atom of the

$(HC_2O_4)^-$ group and the nitrogen atom of $(C_6H_{16}N_2)^{2+}$ correspond to a strong hydrogen bond like O–H...N. This strong attractive interaction has a negative sign $(\lambda 2)\rho$ and is located between –0.04 and –0.05 a.u. Thus, we can conclude that the RDG can be considered as an extension of the AIM analysis for the visual study.

3.10. The NBO Analysis

The NBO analysis was used to determine the electron density distributions in atoms of molecular systems [27]. It allowed us to examine and evaluate the interaction between the non-Lewis acceptor (antibonding) NBOs and the Lewis-type donor (bonding) NBOs within the second-order perturbation theory. We performed the NBO calculation for the 1EPBH compound using the Gaussian package. The higher value of the second-order perturbation interaction energy $E(2)$ indicates that the electron donors and electron acceptors in the molecular system have a great capability of interaction. The perturbation energies $E(2)$ for the donor–acceptor interactions are summarized in **Table S2**. In this system, the stabilization occurs via intermolecular interactions of the orbital overlap among the σ→σ* and LP→ π* orbitals, which results in the intermolecular charge transfer. Meanwhile, the NBO calculation can disclose the presence of hydrogen bonding interactions between oxygen lone electron pairs LP(O) and the antibonding orbital σ*(X–H). These types of hyper-conjugative interactions promote charge transfer and ensure the molecular stability. It can be seen that LP_2 $(O_2)\rightarrow\sigma^*(N_{16}\text{-}H_{17})$ and LP_1 $(N_7)\rightarrow$ $\sigma^*(H_8\text{-}O_{37})$ have high $E(2)$ values (81.99 and 41.14 kcal/mol, respectively). The calculated stabilization energies of the hyper-conjugative interactions LP_1 $(N_7)\rightarrow$ $\sigma^*(C_4\text{-}H_5)$ and LP_1 $(N_7)\rightarrow$ $\sigma^*(C_{10}\text{-}H_{12})$ are 4.63 and 4.42 kcal/mol, respectively. We can conclude that the NBO analysis confirm the existence of the N–H...O and C–H...O intermolecular interactions.

3.11. Atomic Charge Distribution Method

The atomic charge of the investigated compounds was calculated using the GaussView 09 software at the B3LYP 6-311++G(d,p) level. The atomic charge is directly related to the vibrational properties of a molecule and quantifies the way to change the electronic structure in atomic displacement; on the other hand, it is directly related to chemical bonds existing in a molecule. This affects the dipole moment, polarizability, electronic structure, and properties of a molecular system. Atoms presented by different colors according to their Mulliken charges and a graph are shown in **Figure S10**. The color gradient in the figure is used to determine the color of each atomic charge and varies from red (more electronegative) to blue (less electronegative) through brown with a range from –0.707 to 0.707 (from more electronegative

colored in red to less electronegative colored in green). In addition, the atomic charge distributions for different atoms in the investigated compound are shown in **Figure S11** and summarized in **Table S3**. The charge distribution shows that the carbon atoms attached to an oxygen atom are charged positively (except for the C26 atom), while the other carbon atoms are charged negatively and all hydrogen atoms are charged positively. The N7 and N16 nitrogen atoms are the most negatively charged, which shows the H-to-N charge transfer. The maximum atomic charge is obtained for the C_{28} and C_{36} atoms. This is due to the attachment of carbon between two negatively charged atoms (C_{28} between O_{30} and O_{29} and C_{36} between O_{37} and O_{38}). Furthermore, the hydrogen atoms attached to the N or O atoms (NH and OH) have larger positive atomic charges than the other hydrogens (H_{17} and H_8). The strong negative charges are noticed in oxygen atoms, which are involved, as acceptors, in hydrogen bonds.

3.12. Vibrational Analysis

In this Section, the vibrational assignments of all bands of the compound under study were made and determined. **Figure 8** shows the experimental and theoretical infrared spectra between 4000 and 500 cm^{-1} for 1-ethylpiperazine-1,4-diium bis(hydronenoxalate). However, on the basis of the XRD data, the molecular vibrational frequencies of the 1EPBH compound were found using the DFT/B3LYP/6-311++G(d, p) level of theory. The molecule used in the calculation is that of the asymmetric unit. The calculation yielded the results much more convincing in terms of numbers and positions of the bands, since there are no imaginary frequencies. The experimental and calculated infrared spectra are similar and demonstrate good agreement between the experimental and theoretical data (**Figure S12**). In the figure, the scale bill is 0.964. The vibrations of the C-H bond are found in the spectrum around 3000 cm-1 [4]. In the case of the piperazine cycle, the smaller the size, the more the frequencies of the CH_2 bands increase and the intensities decrease. For the δ(C-H) deformation mode, it is localized around 880-720 cm-1 and according to the number of substituents. We can know the OH group by the existence of a hydrogen bond between H and another oxygen atom. The spectrum is characterized by a band that is so lowered and widened that it overlaps the ν(CH) bands. These widths can give information about the strengths of the hydrogen bonds [42-43]. The ν(OH) band and the ν(NH) band are very close but the latter is narrower and is indicated in the form of a doublet (symmetrical and asymmetrical vibration) when it comes to NH2 or NH3.The strongly bound O-H group is located in the range 2500-1600 cm^{-1}. In the simulated IR spectra, the band at 1730 cm^{-1} corresponds to the vibration of the C=O group, while the asymmetric and symmetric elongation vibrations of COO^- occur around 1530 and 1405 cm^{-1}, respectively.

These values are consistent with the experiment. The theoretical band at 1262 cm^{-1} corresponds to the C–N and C–O asymmetric stretching vibrations, while the band at 1048 cm^{-1} corresponds to the C–N symmetric vibration. The two experimental bands at 1200 and 1048 cm^{-1} are related to the asymmetric and symmetric C–C vibrations. A series of bands at 802, 702, and 548 cm^{-1} correspond to the δ(COH), δ(COO^{-}), and δ(CCN) bending vibrations, respectively. It should be noted that the theoretical calculation reproduces sufficiently well the same experimental observations, since the characteristic vibrational modes of each grouping yielded by the calculation are very close to those in the experimental spectrum (**Table S4**).

3.13. UV-Visible Spectroscopy

The UV-Visible spectrum of 1-Ethylpiperazine-1,4-diium bis (hydrogenoxalate) was recorded between 200 and 400 nm (**Figure 9.a**). The analysis of this spectrum shows a single intense band with a maximum at 274 nm, which can be attributed to the n→π* transition of the carbonyl group of the carboxyl function. The absorption is low, which allows the transmission of a laser beam; in addition, this material has a high transparency in the UV and visible range and can therefore be used in nonlinear optics. In addition, the UV-Visible spectrophotometry study allowed us to determine the HOMO–LUMO energy gap E_g. The optical gap E_g is determined from the formula proposed by Tauc [44]:

$$(\alpha .h\nu)2 = (h\nu - E_g) \quad (1)$$

Using the Tauc method, we found the gap energy for the investigated compound: 5.47 eV (**Figure.9.b**). This is similar with the values found in the FMO (HOMO–LUMO) analysis. Such a wide gap suggests that this material has a high transmittance in the visible range.

3.14. NMR Study of 1-Ethylpiperazine-1,4-diium bis (hydrogenoxalate)

The asymmetric unit of the 1EPBH compound contains ten carbon atoms. The NMR spectrum of carbon ^{13}C decoupled from the proton (**Figure S13**) includes ten lines. Four lines located in the resonance region between 9.5–28 ppm are assigned to carbon atoms of the crystallographic-independent carbonyl groups 2 C_2HO_4. Six lines with the chemical shifts distributed between 132.17 ppm and 177 ppm are caused by the presence of crystallographic-independent organic group atoms. These results prove that the asymmetric unit contains one organic cation and two oxalate anions and agree well with the crystallographic data. In addition, **figure S13** shows the numbering of carbon atoms of the asymmetric unit. The theoretical and experimental chemical shifts of carbon atoms in the 1EPBH molecule (**Table 5**) were made at the B3LYP/6-311++G(d, p) level of theory. The difference between the experimental and theoretical chemical shifts is due to the fact that the spectrum was recorded in the solid state,

while the theoretical chemical shift corresponds to an isolated molecule of the compound. **Figure S14** shows the graphical correlation between the experimental and theoretical chemical shifts. Further, **Figure S15** showing the ^{1}H proton spectrum of the investigated compound confirms the XRD data. Indeed, this spectrum contains 18 lines of H protons, which is consistent with 18 hydrogen atoms in the asymmetric unit.

4. Molecular Docking Study

To examine the biological activity of the molecule under study, we performed the molecular docking calculation. To do that, 1EPBH was submitted to the Swiss Target Prediction Server, which specified the compound could target carbonic anhydrase VII, carbonic anhydrase IX, and carbonic anhydrase XII. These proteins are related to the epilepsy and cancer diseases [45–47]. To test the Swiss Target prediction data, the molecular docking calculation was performed. The RCSB protein data bank was used to get a 3D crystal structure of the receptor applied for docking assessment (Carbonic anhydrase VII: PDB ID: 3MDZ and 6H36, Carbonic anhydrase IX: PDB ID:5FL5, and Carbonic anhydrase XII: PDB ID: 1JCZ). The redocking protocol was performed using the MOE program in the binding site of the enzymes (**Figure 10**). The 2D and 3D representation of the investigated compound (ligand) with different receptors allows one to find active sites. **Figure 10** indicates the top conformation, which corresponds to the shortest energy of each of the 3MDZ–1EPBH, 1JCZ–1EPBH, 5FL5–1EPBH, and 6H36–1EPBH complexes. Furthermore, the binding score, root-mean-square deviation (RMSD), and bonds between atoms of the compounds and residues of active sites were computed and summarized in **Table 6**. The best configuration is the one with a small binding score (kcal/mol). This score is the total energy consumed for the formation of bonding interactions between the ligand (1EPBH) and chosen proteins. In addition, the ability of the program to determine the correct position of the ligand relative to its protein is determined generally by the root-mean-square deviation (RMSD). The docking results are considered to be reliable when the accepted RMSD value is a maximum difference of 2 A° (beyond the prediction considered as inadequate) [48, 49]. In this context, according to **table 6**, all the examined complexes yielded good docking results. The binding scores values for 3MDZ, 1JCZ, 5FL5 and 6H36 are –3.15 kcal/mol, –5.36 kcal/mol, –3.69 kcal/mol, and –3.92 kcal/mol, respectively. In addition, the RMSD values of these complexes range from 1.40 A° to 2.01 A°. The data given in **table 6** showed that the key amino acids contributing to the 1EPBH ligand with the target receptors are TYR, LYS, CYS, THR, and HIS and their distance ranges between 2.74 A° and 4.35 A°. The smaller distance proves the strength of the established H bonds. In

3MDZ–1EPBH, O32 and O33 of the hydrogenoxalate group are involved, together with TYR9 and LYS101, in the H donor and H acceptor with distances of 2.74 A° and 3.07 A°, respectively. 1JCZ-1EPBH shows two involved receptor residues of CYS232 and TYR 7 in the H donor and H acceptor at distances of 3.62 A° and 3.04 A°. Similarly, the 5FL5 docked conformation is involved, together with CYS232 and TYR7, in the H donor and H acceptor. For the 1-EPBH-6H36 interaction, three conventional hydrogen bonds are formed between O31, O36, and C1 and amino acids THR199, THR99, and 5-RING HIS 94 H-donor (3.08 A°), H-acceptor (2.90 A°), and H-pi bond (4.35 A°), respectively. All these interactions allow the stabilization of a ligand at the protein active sites. Thus, according to the results obtained, we can conclude that our compound (chosen as a ligand) can be an important epilepsy and cancer inhibitor.

5. Conclusions

In this study, the structure of the 1EPBH compound was investigated using the DFT/B3LYP/6-311++G(d, p) for the gas phase and the IEFPCM method for the solvent (water and DMSO) phase. We find that the value of dipole moment of the DMSO is small compared than water. This is explains that the DMSO is capable for accepting hydrogen bonds. Further, It was shown that the solvent (water and DMSO) increases the O...H distance.

The convergence and stability of the investigated compound were confirmed by the ADMP molecular dynamic simulation. Further, the effect of a solvent on the electronic proprieties (FMO and MEPS) was exactly determined. It was demonstrated using the AIM, ELF, LOL, and ALIE topological analysis that two types of hydrogen bonds (weak and medium) are ensured between the organic and inorganic groups of the 1EPBH molecule. The Hirshfeld surface analysis indicates that the most important contribution for the crystal packing is from O...H/H...O, suggesting the presence of C–H...O and N–H...O hydrogen bonds. The RDG approach point out the different weak interactions within our compound such as the hydrogen bonding, vdw interactions and steric effect. Further, the NBO analysis is achieved to estimate the transfer of charge in terms of 'donor-acceptor' within the molecule 1EPBH. The atomic charge analyses determine the nature and proprieties of molecular interactions of the 1EPBH molecule. Using the vibrational analysis, it was found that the theoretical calculation reproduces sufficiently well the same experimental observations, since the characteristic vibrational modes of each grouping yielded by the calculation are similar to those observed in the experimental spectrum. In addition, the UV-Visible and ^{13}C and ^{1}H NMR analysis was performed. Finally, it was confirmed using the molecular docking that the investigated compound (chosen as a ligand) can serve as an important epilepsy and cancer inhibitor.

Acknowledgements.

This work were supported by the Tunisian National Ministry of Higher Education and Scientific Research and Researchers Supporting Project number (RSP-2021/61), King Saud University, Riyadh, Saudi Arabia.

References

[1] S. Gatfaoui, A. Sagaama, N. Issaoui, T. Roisnel, H. Marouani, Synthesis, experimental, theoretical study and molecular docking of 1-ethylpiperazine-1, 4-diium bis (nitrate). Solid State Sciences, 106 (2020) 106326. https://doi.org/10.1016/j.solidstatesciences.2020.106326

[2] M. Berkheij, L. van der Sluis, C. Sewing, D. J. den Boer, J. W. Terpstra, H. Hiemstra, Synthesis of 2-substituted piperazines via direct α-lithiation. Tetrahedron Letters, J. H. van Maarseveen, 46(14) (2005) 2369-2371. https://doi.org/10.1016/j.tetlet.2005.02.085

[3] O. Noureddine, N. Issaoui, S. Gatfaoui, O. Al-Dossary, H. Marouani, Quantum chemical calculations, spectroscopic properties and molecular docking studies of a novel piperazine derivative, Journal of King Saud University-Science, 33(2) (2021) 101283. https://doi.org/10.1016/j.jksus.2020.101283

[4] O. Noureddine, S. Gatfaoui, S. A. Brandán, H. Marouani, N. Issaoui Structural, docking and spectroscopic studies of a new piperazine derivative, 1-Phenylpiperazine-1, 4-diium bis (hydrogen sulfate), Journal of Molecular Structure, 1202 (2020) 127351. https://doi.org/10.1016/j.molstruc.2019.127351

[5] R. S. Upadhayaya, S. Jain, N. Sinha, N. Kishore, R. Chandra, S. K. Arora, Synthesis of novel substituted tetrazoles having antifungal activity. European journal of medicinal chemistry, 39(7) (2004) 579-592. https://doi.org/10.1016/j.ejmech.2004.03.004

[6] D. G. Michael, P. Adamson, T. Alexopoulos, W. W. M. Allison, G. J. Alner, K. Anderson, J. McDonald, Observation of muon neutrino disappearance with the MINOS detectors in the NuMI neutrino beam. Physical review letters, 97(19) (2006) 191801. https://doi.org/10.1103/PhysRevLett.97.191801

[7] S. D. Archana, H. K. Kumar, H. S. Yathirajan, S. Foro, M. S. Abdelbaky, S. Garcia-Granda, Crystal structure studies of 4-ethylpiperazin-1-ium 3, 5-dinitrobenzoate, 4-methylpiperazin-1-ium 3,5-dinitrobenzoate and 4-methylpiperazin-1-ium 4-iodobenzoate. ActaCrystallographica Section E: Crystallographic Communications, 77(11) (2021) 1. https://doi.org/10.1107/S2056989021010689

[8] Bruker APEX2, SAINT and SADABS. Bruker AXS Inc., Madison, Wisconsin, USA (2006).

[9] G. M. Sheldrick, SHELX-97, Program for solution of Crystal Structures. University of Göttingen,Germany, (1997).

[10] L. J. Farrugia WINGX, A MS-Windows System of Programs for Solving, Refining and Analysing Single Crystal X-ray Diffraction Data for Small Molecules (University of Glasgow, Glasgow, 2005).

[11] K. Brandnburg, Diamond Version 2.0, (1998).

[12] L. J. Farrougia, J. Appl. Cryst., 30 (1997) 565.

[13] A. Frisch, gaussian 09W Reference. Wallingford, USA, 25p (2009) 470.

[14]] R. Dennington, T. Keith, J. Millam, GaussView, Version 5, Semichem. Inc, I. Jomaa et al. / Journal of Molecular Structure 1213 (2020) 128186 13 Shawnee Mission, KS, 2009. https://doi.org/10.1016/j.molstruc.2020.128186

[15] N.M. O'Boyle, A.L. Tenderholt, K.M. Langer, A library for package independent computational chemistry algorithms, J. Comput. Chem., 29 (2008) 839e845. https://doi.org/10.1002/jcc.20823

[16] T. Lu, F. Chen, Multiwfn: a multifunctional Wavefunction analyzer, J. Comptu. Chem. 33 (2012) 580e592. https://doi.org/10.1002/jcc.22885

[17]T. A. Keith, AIMAll, Version 10.05.04 (TK Gristmill Software, Overland Park KS, USA, 2010). aim.tkgristmill.com.

[18] S.K. Wolff, D.J. Grimwood, J.J. McKinnon, M.J. Turner, D. Jayatilaka, M.A. Spackman, Crystal Explorer (Version 3.1), UWA, 2012.

[19] C. D. Schwieters, G. M. Clore, The VMD-XPLOR visualization package for NMR structure refinement. Journal of Magnetic Resonance, 149(2) (2001) 239-244. https://doi.org/10.1006/jmre.2001.2300

[20] http://www.rcsb.org/pdb/

[21] Molecular Operating Environment (MOE), 2015.10; Chemical Computing Group Inc., 1010 Sherbooke St. West, Suite #910, Montreal, QC, Canada, H3A 2R7, 2015. https://doi.org/10.4155/fmc-2022-0067

[22] I. D, Brown. ActaCrystallogr., A32 (1976) 24. https://doi.org/10.1107/S0567739476000041

[23] H. B. Schlegel, et al. Ab initiomolecular dynamics: Propagating the density matrix with Gaussian orbitals. The Journal of Chemical Physics 114 (2001) 9758–9763. https://doi.org/10.1063/1.1372182

[24] H. B. Schlegel, et al. Ab initio molecular dynamics: Propagating the density matrix with Gaussian orbitals. III. Comparison with Born–Oppenheimer dynamics. The Journal of Chemical Physics 117 (2002) 8694–8704. https://doi.org/10.1063/1.1514582

[25] N. Rega, et al. Hybrid ab-initio/empirical molecular dynamics: combining the ONIOM scheme with the atom-centered density matrix propagation (ADMP) approach. 108 (2004) 4210–4220. https://doi.org/10.1021/jp0370829

[26] S. S. Iyengar, H. Bernhard Schlegel, G. A. Voth, Atom-Centered Density Matrix Propagation (ADMP): Generalizations Using Bohmian Mechanics †. Journal of Physical Chemistry A - J Phys Chem A 107 (2003). https://doi.org/10.1021/jp034633m

[27] S. Gatfaoui, N. Issaoui, S. A. Brandán, M. Medimagh, O. Al-Dossary, T. Roisnel, A. S. Kazachenko, Deciphering non-covalent interactions of 1, 3-Benzenedimethanaminium bis (trioxonitrate): Synthesis, empirical and computational study. Journal of Molecular Structure, 1250 (2022) 131720. https://doi.org/10.1016/j.molstruc.2021.131720

[28] I. Jomma, N. Issaoui, T. Roisnel, H. Marouani, Insight into non-covalent interactions in a tetrachlorocadmate salt with promising NLO properties: Experimental and computational analysis, J. Mol. Structure,1242 (2021) 130730. DOI:10.1016/j.molstruc.2021.130730.

[29] J. Bevanott, Calculations From Statistical Thermodynamics, Academic press, 2000.

[30] R. Zhang, B. Dub, G. Sun, Y. Sun, Spectrochim. Acta A., 75 (2010) 1115–1124. https://doi.org/10.1016/j.saa.2009.12.067

[31] T. Fradi, O. Noureddine, F. B. Taheur, M. Guergueb, S. Nasri, N. Amiri,, H. Nasri, New DMAP meso-arylporphyrin Magnesium (II) complex. Spectroscopic, Cyclic voltammetry and X-ray molecular structure characterization. DFT, DOS and MEP calculations and Antioxidant and Antifungal activities. Journal of Molecular Structure, 1236 (2021) 130299. https://doi.org/10.1016/j.molstruc.2021.130299

[32] A. Kazachenko, F. Akman, M.Medimagh, N.Issaoui, N. Vasilieva, Y. N.Malyar,O. M. Al-Dossary, Sulfation of Diethylaminoethyl-Cellulose: QTAIM Topological Analysis and Experimental and DFT Studies of the Properties. ACS omega, 6(35) (2021) 22603-22615. https://doi.org/10.1021/acsomega.1c02570

[33] M.Harzallah, M. Medimagh, N.Issaoui, T. Roisnel, A. Brahim, Synthesis, X-ray crystal structure, Hirshfeld surface analysis, DFT, AIM, ELF, RDG and molecular docking studies of bis [4-(dimethylamino) pyridinium] di-μ-chlorido-bis [dichloridomercurate (II)]. Journal of Coordination Chemistry, 74(17-20) (2022) 2927-2946. https://doi.org/10.1080/00958972.2021.2006649

[34] M. Medimagh, N. Issaoui, S. Gatfaoui, O. Al-Dossary, A. S. Kazachenko, H. Marouani, M. J. Wojcik, Molecular modeling and biological activity analysis of new organic-inorganic hybrid: 2-(3, 4-dihydroxyphenyl) ethanaminium nitrate. Journal of King Saud University-Science, 33(8) (2021) 101616. https://doi.org/10.1016/j.jksus.2021.101616

[35] M. Medimagh, N. Issaoui, S. Gatfaoui, S. A. Brandán, O. Al-Dossary, H. Marouani, M. J. Wojcik, Impact of non-covalent interactions on FT-IR spectrum and properties of 4-methylbenzylammonium nitrate. A DFT and molecular docking study. Heliyon, 7(10) (2021) e08204. https://doi.org/10.1016/j.heliyon.2021.e08204

[36] A. S. Kazachenko, M. Medimagh, N. Issaoui, O. Al-Dossary, M. J. Wojcik, A. S. Kazachenko, Y. N. Malyar, Sulfamic acid/water complexes (SAA-H2O (1-8)) intermolecular hydrogen bond interactions: FTIR, X-ray, DFT and AIM analysis. Journal of Molecular Structure, (2022) 133394. https://doi.org/10.1016/j.molstruc.2022.133394

[37] T. Pooventhiran, M. Cheriet, U. Bhattacharyya, A. Irfan, R. Puchta, S. Sowrirajan, R. Thomas, Detailed Structural Examination, Quantum Mechanical Studies of the Aromatic Compound Solarimfetol and Formation of Inclusion Compound with Cucurbituril. Polycyclic Aromatic Compounds, (2021) 1-13. https://doi.org/10.1080/10406638.2021.1937238

[38] N. Elangovan, A. Latha, V. Maheswari, K. P. Manoj, S. Chandrasekar, Synthesis, Single Crystal (Xrd), Spectral Characterization (Ft-Ir, Ft-Raman, 1hnmr, 13cnmr, 119sn Nmr), Computational (Dft), Quantum Chemical Modeling and Anticancer Activity Studies of Di (P-Bromobenzyl)(Dibromo)(1, 10-Phenanthroline) Tin (IV) Complex. Computational (Dft), Quantum Chemical Modeling and Anticancer Activity Studies of Di (P-Bromobenzyl)(Dibromo)(1, 10-Phenanthroline) Tin (IV) Complex. https://doi.org/10.1016/j.jics.2022.100714

[39] A. S. Kazachenko, N. Issaoui, M. Medimagh, O. Y. Fetisova, Y. D. Berezhnaya, E. V. Elsuf'ev, L. G. Bousiakou, Experimental and theoretical study of the sulfamic acid-urea deep eutectic solvent. Journal of Molecular Liquids, 363 (2022) 119859. https://doi.org/10.1016/j.molliq.2022.119859

[40] O.Noureddine, N.Issaoui, M.Medimagh, O.Al-Dossary,H.Marouani, Quantum chemical studies on molecular structure, AIM, ELF, RDG and antiviral activities of hybrid hydroxychloroquine in the treatment of COVID-19: Molecular docking and DFT calculations. Journal of King Saud University-Science, 33(2) (2021) 101334. https://doi.org/10.1016/j.jksus.2020.101334

[41] A.Sagaama, N.Issaoui, O.Al-Dossary, A. S. Kazachenko, M. J. Wojcik, Non covalent interactions and molecular docking studies on morphine compound. Journal of King Saud University-Science, 33(8) (2021) 101606. https://doi.org/10.1016/j.jksus.2021.101606

[42] I. Matulkova´, I. Němec, K. Teubner, P. Němec & Z. Mička, J. of Mol. Struct., 873, 46–60 (2008). https://doi.org/10.1016/j.molstruc.2007.03.007

[43] N. Rekik, N.Issaoui, B. Oujia, M.J.Wójcik, Theoretical IR spectral density of H-bond in liquid phase: Combined effects of anharmonicities, Fermi resonances, direct and indirect relaxations, Journal of Molecular Liquids, 141, 3,(2008) 104 – 109. DOI:10.1016/j.molliq.2007.10.009

[44] J. Tauc, Mater. Res. Bull., 3 (1968) 37. https://doi.org/10.1016/0025-5408(68)90023-8

[45] M. Benej, S. Pastorekova, J. Pastorek, Carbonic anhydrase IX: regulation and role in cancer. Carbonic anhydrase: mechanism, regulation, links to disease, and industrial applications, 199-219 (2014). DOI: 10.1007/978-94-007-7359-2_11.

[46] S. Pastorekova, R. J. Gillies, The role of carbonic anhydrase IX in cancer development: links to hypoxia, acidosis, and beyond. Cancer and Metastasis Reviews, 38(1) (2019) 65-77. https://doi.org/10.1007/s10555-019-09799-0

[47] M. R. Buemi, A. Di Fiore, L. De Luca, A. Angeli, F. Mancuso, S. Ferro, R. Gitto, Exploring structural properties of potent human carbonic anhydrase inhibitors bearing a 4-(cycloalkylamino-1-carbonyl) benzenesulfonamide moiety. European journal of medicinal chemistry, 163 443-452. https://doi.org/10.1016/j.ejmech.2018.11.073

[48] M. Kontoyianni, L. M. McClellan, G. S. Sokol, Evaluation of docking performance: comparative data on docking algorithms. Journal of medicinal chemistry, 47(3) (2004) 558-565. https://doi.org/10.1021/jm0302997

[49] A. Ramalingam, S. Sambandam, M. Medimagh, O. Al-Dossary, N. Issaoui,M J. Wojcik, Study of a new piperidone as an anti-Alzheimer agent: Molecular docking, electronic and intermolecular interaction investigations by DFT method. Journal of King Saud University-Science, 33(8) (2021) 101632. https://doi.org/10.1016/j.jksus.2021.101632

Author statements

Mouna Medimagh: Conceptualization, Methodology, Investigation, Writing – original draft.

Cherifa Ben Mleh: Methodology, Investigation, Formal analysis and Writing.

Noureddine ISSAOUI: Writing – review & editing, Supervision, Visualization.

Aleksandr S. Kazachenko: Methodology, Investigation.

Thierry Roisnel: Investigation, Software.

Omar M. Al-Dossary: Methodology, Investigation.

Houda MAROUANI: Investigation, Writing – original draft, Methodology.

Leda G. Bousiakou: Investigation

Highlights

- The molecular structure in the gas, water, and DMSO has been studied using the DFT/B3LYP/6-311++G(d,p).
- The effect of a solvent on the electronic proprieties (FMOs and MEPS) has been investigated.
- The weak interactions in the 1EPBHcompound have been established by different methods (AIM, ELF, LOL, etc.).
- The FT-IR, RMN, and UV-visible studies and molecular docking have been found and analyzed.

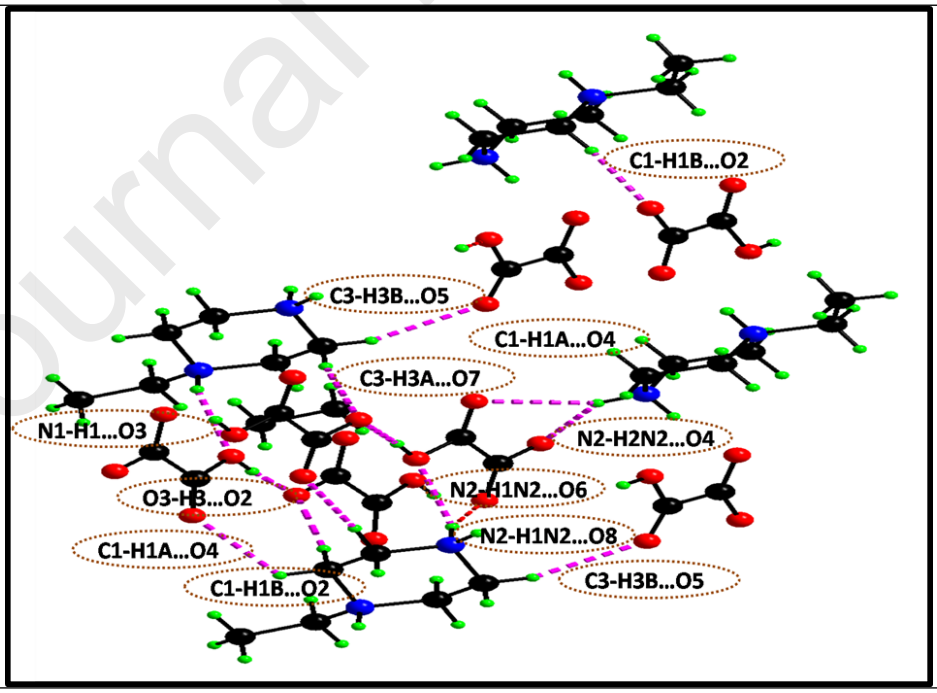

Figure 1: Hydrogen bonds in the [C6H16N2](HC2O4)2 structure.

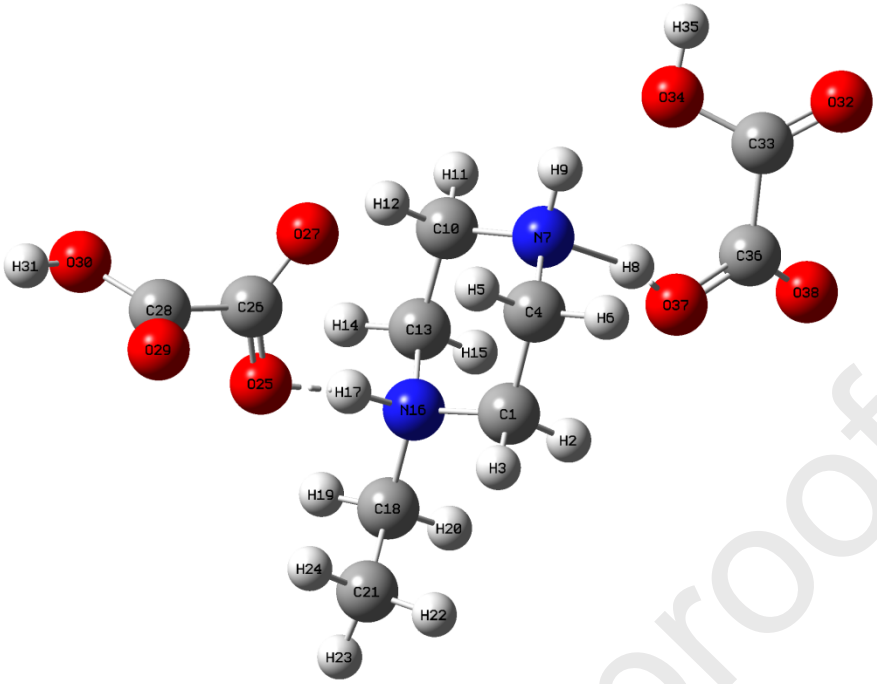

Figure 2: Optimized molecular structure of the 1EPBH compound in the gas phase.

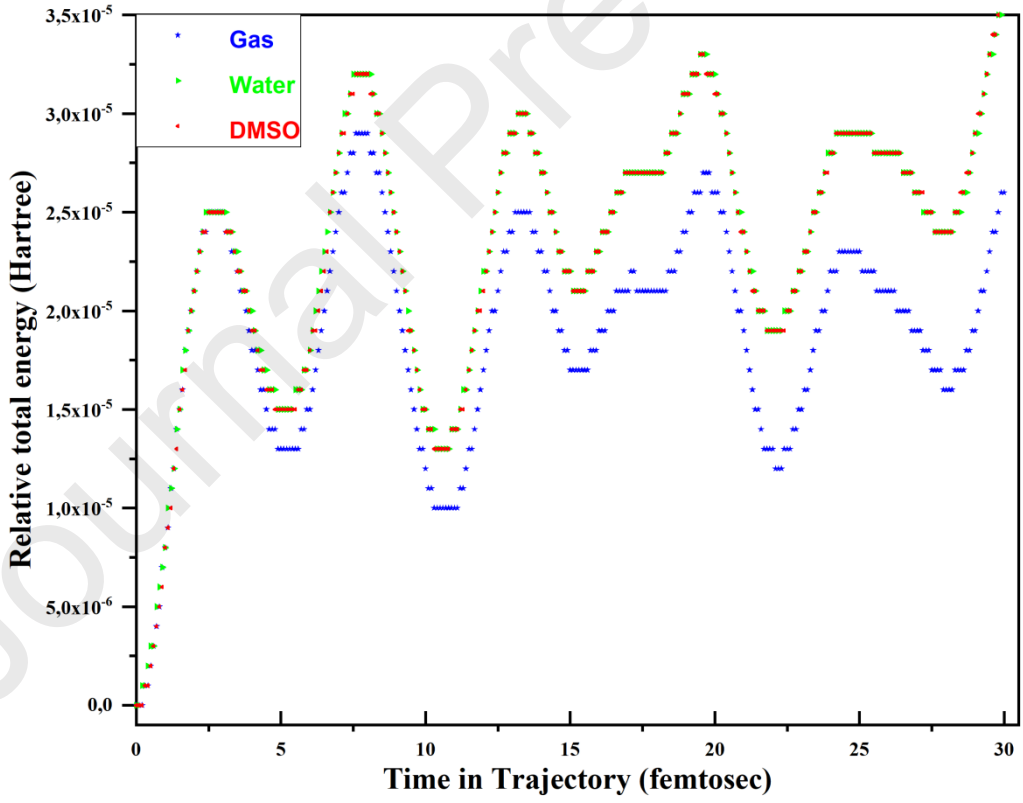

Figure 3: ADMP trajectory of the 1EPBH compound in different phases (gas, water, and DMSO).

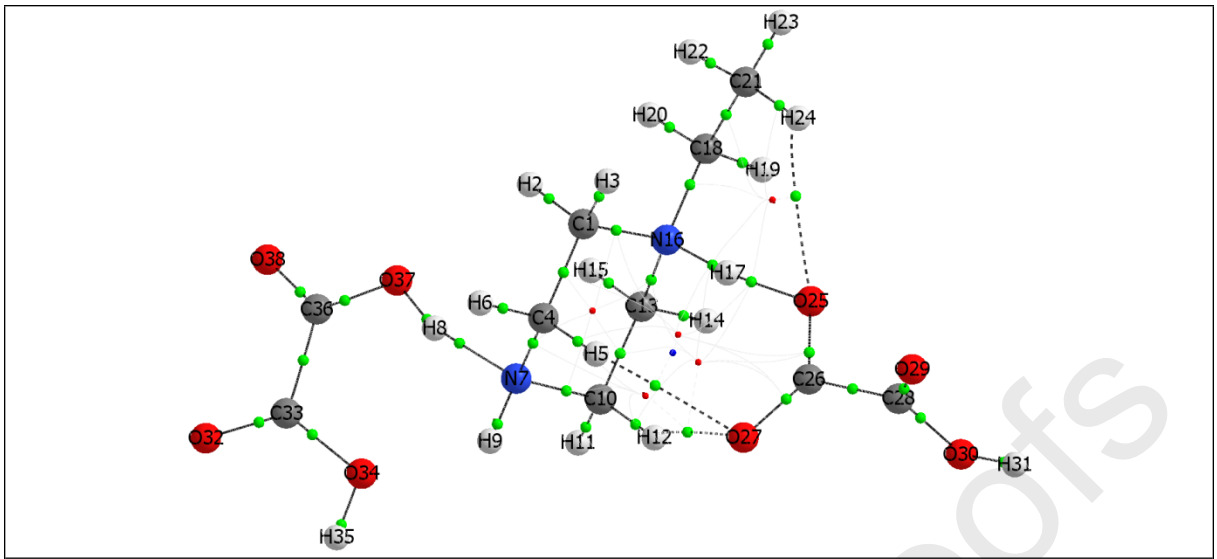

Figure 4: AIM structure of the 1EPBH compound.

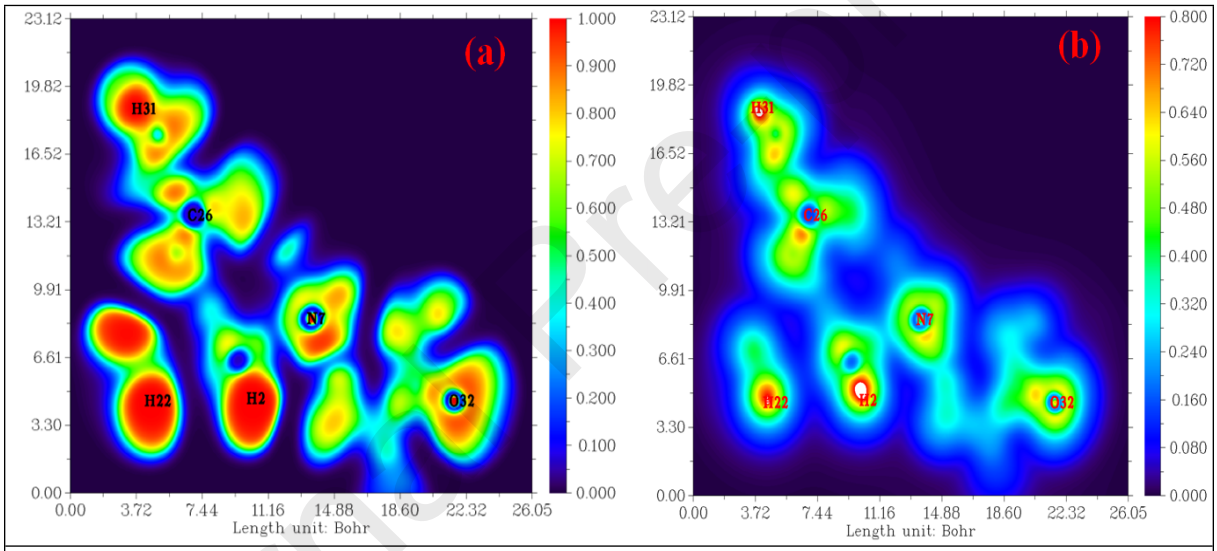

Figure 5: (a) ELF and **(b)** LOL plots of the 1EPBH molecule.

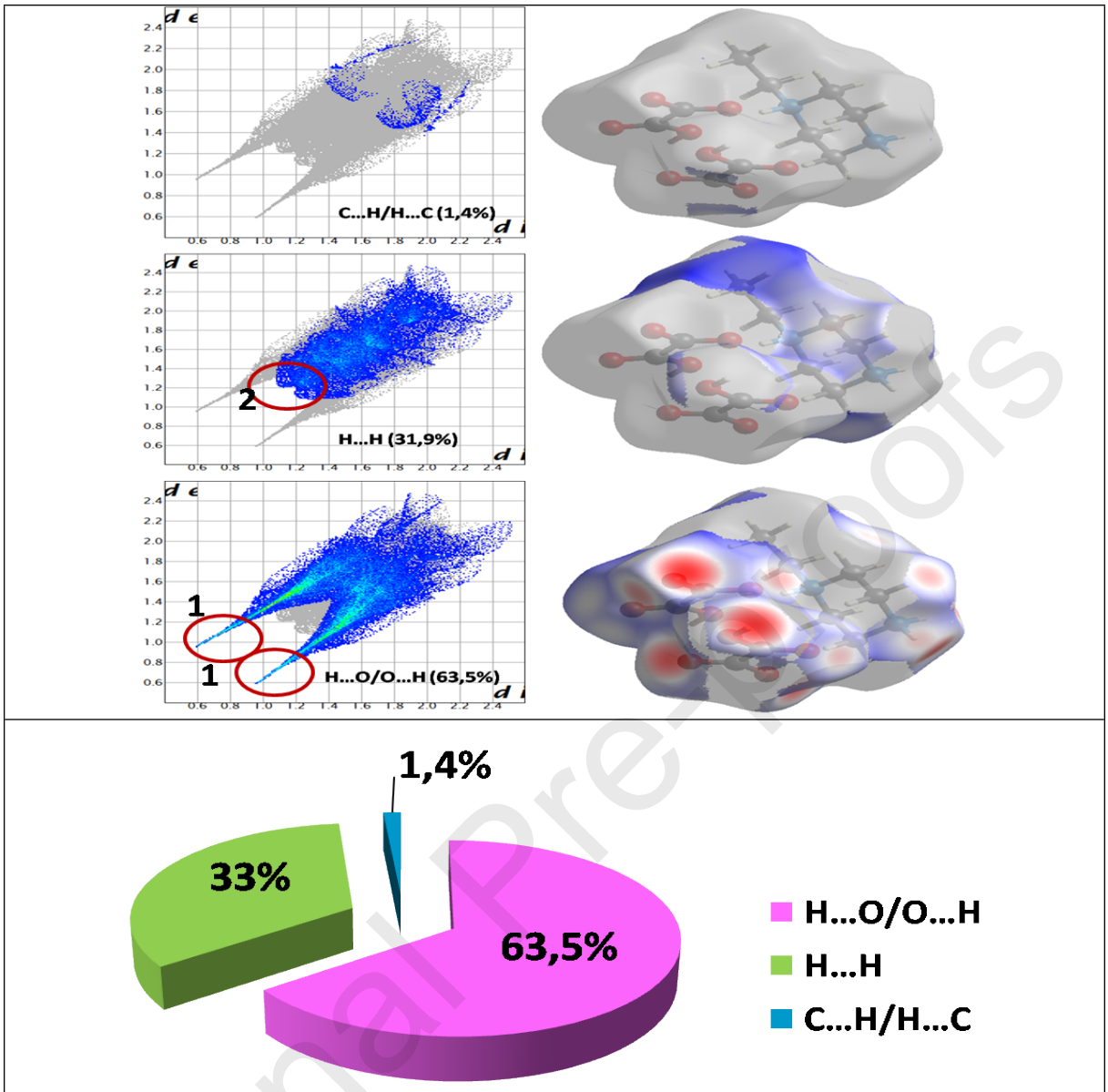

Figure 6: (a) Couples pairs *d*i and *d*e of the interatomic contacts and **(b)** relative contributions of different intermolecular Hirshfeld surface interactions in the 1EPBH compound.

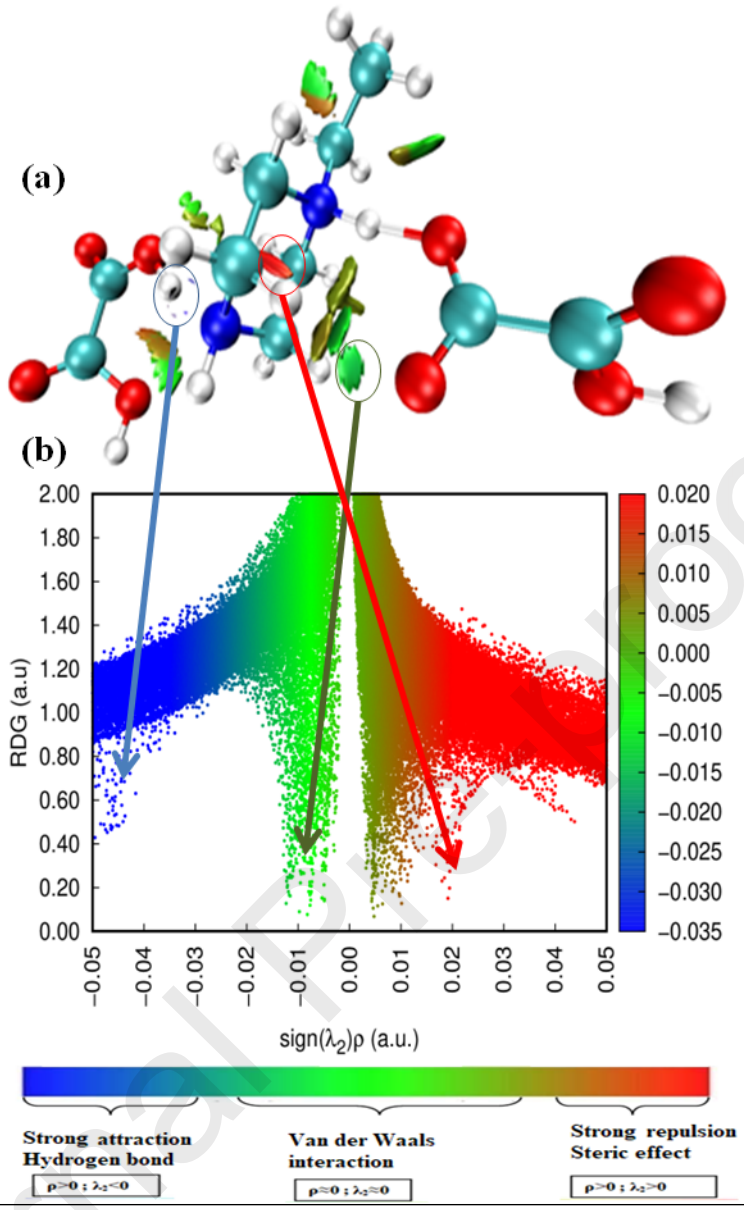

Figure 7: (a) 2D plot and **(b)** RDG versus sign (λ_2)ρ of the 1EPBH molecule.

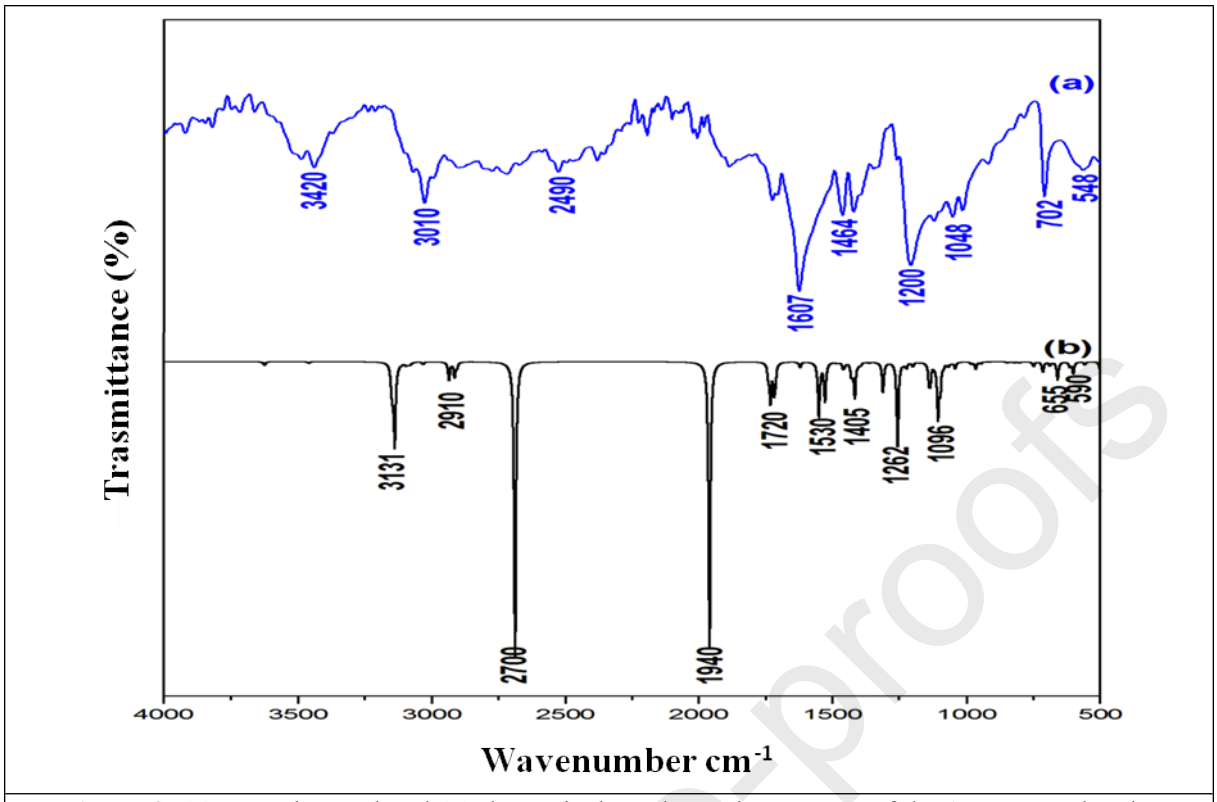

Figure 8: **(a)** Experimental and **(b)** theoretical IR absorption spectra of the 1EPBH molecule.

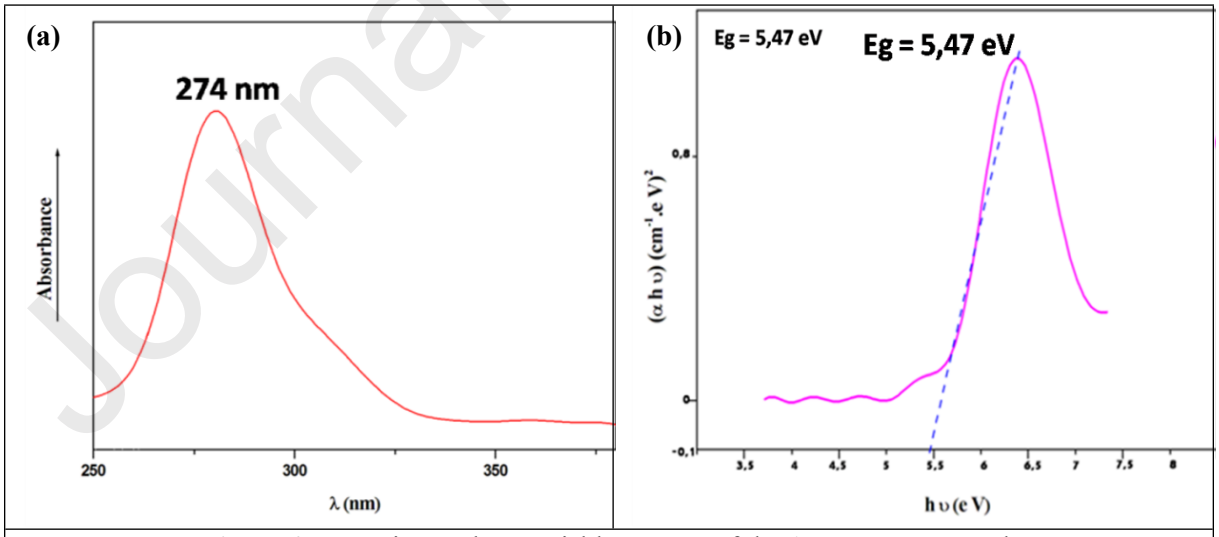

Figure 9: Experimental UV-Visble spectra of the 1EPBH compound.

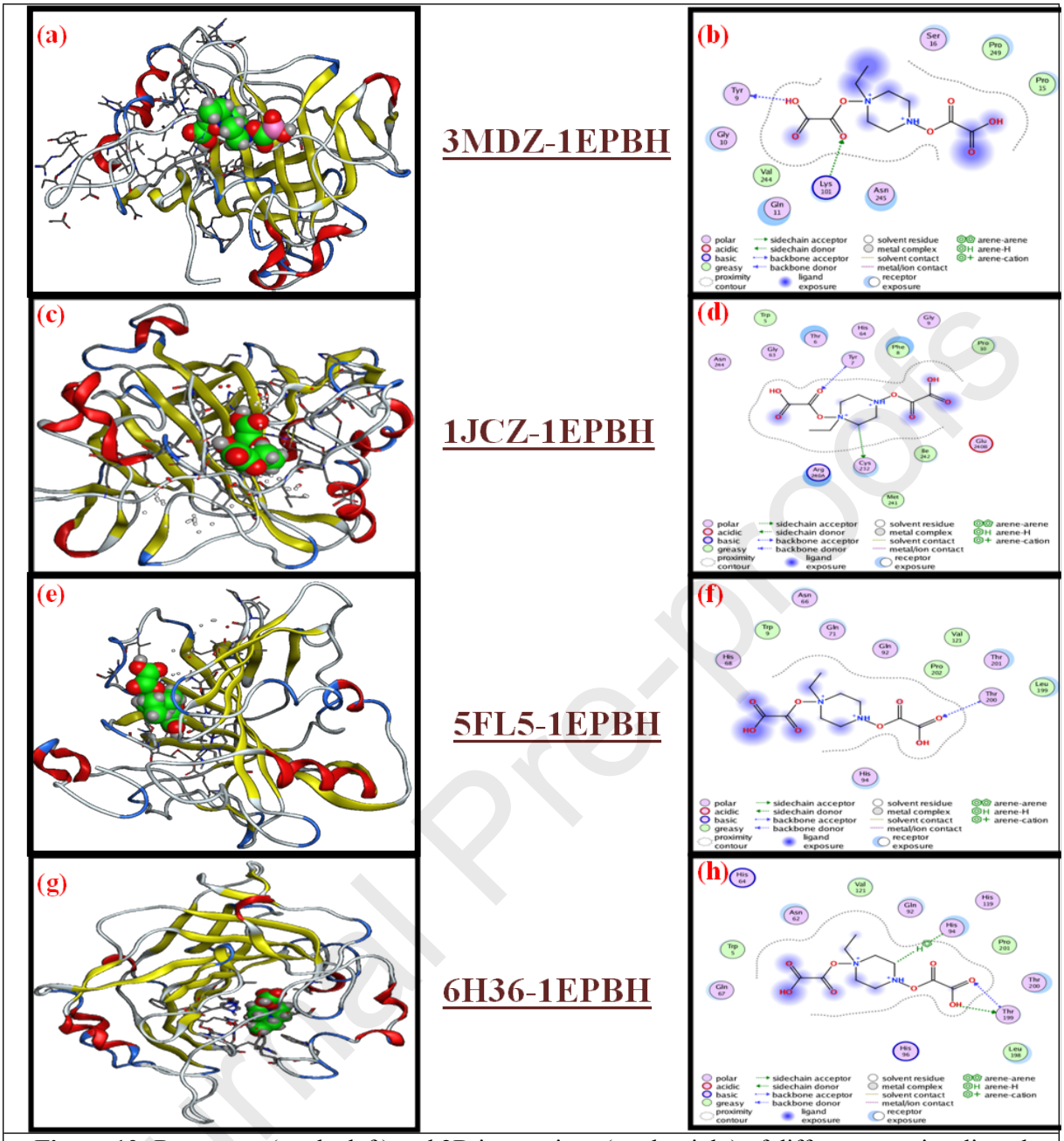

Figure 10: Best poses (on the left) and 2D interactions (on the right) of different proteins–ligand complexes.

Table 1: Crystallographic, intensity measurement, and structural data for the 1EPBH compound

Crystallographic data	
Formula: $C_6H_{16}N_2(HC_2O_4)_2$	System: monoclinic
Molecular weights: 294.26 g.mol^{-1}	Space group: C2/c
a = 15.6403(14) Å, b = 5.6682(6) Å, c = 29.901(3) Å, β =103.649(3) Å	
V = 2575.9(4) Å^3	Z = 8
ρ_{cal} = 1.518 g.cm^{-3}	F(000) =1248
μ(MoKα) = 0.13 mm^{-1}	crystal size: 0.48 × 0.22 × 0.07 (transparent)

Intensity measurement	
Temperature: 150 K Diffractometer: Bruker D8 VENTURE AXS Domain of measures: $h = -20 \rightarrow 20$, $k = -7 \rightarrow 5$, $l = -38 \rightarrow 38$ Number of independent reflections: 2910 (R_{int} = 0.054)	Wave length: MoK$\overline{\alpha}$ (0.71073Å) $2.7 < \theta < -27.5°$ Total number of reflections: 17058
Structure determination	
Program used: WinGX Single reflections included: 2513 with $I > 2s(I)$ $T_{min} = 0.776$, $T_{max} = 0.991$ $(\Delta/\sigma)_{max} < 0.001$	Direct methods: SHELXL-97 Residual Fourier density: $-0.31 < \Delta\rho < 0.44$ e Å^{-3} Reliability factors: R / RW(F2) = 0.054/0.150 Drawing software: Diamond/Ortep

Table 2: Geometric characteristics of hydrogen bonds in the $(C_6H_{16}N_2)(HC_2O_4)_2$ structure

D—H···A	D—H(Å)	H···A(Å)	D···A(Å)	D—H···A(°)
O3- H3··· O2^{i}	0,82	1.70	2.516(2)	170.7
O6 -H6··· O7^{ii}	0,82	1.73	2.538(2)	170.2
N1 -H1 ···O1	0.89(2)	1.92(2)	2.754(2)	156(2)
N1 -H1 ···O3	0.89(2)	2.30(2)	2.910(2)	125.7(18)
N2-H1N2 ···O8^{iv}	0.90(3)	1.91(3)	2.762(2)	159(2)
N2-H1N2··· O6^{iv}	0.90(3)	2.34(2)	2.929(2)	123(2)
N2-H2N2··· O7^{iv}	0.94(3)	1.97(3)	2.7904(19)	144(3)
N2-H2N2··· O5^{iv}	0.94(3)	2.47(3)	3.244(2)	140(2)
C1-H1A ···O4^{v}	0.97	2.56	3.137(2)	118.2
C1-H1B ···O2^{IV}	0.97	2.24	3.192(2)	167.9
C2-H2A··· O8^{v}	0.97	2.40	3.352(2)	165.2
C3-H3A ···O7	0.97	2.29	3.233(2)	165.0
C3-H3B ···O5^{vi}	0.97	2.48	3.414(2)	161.4
C4 -H4B ···O1^{i}	0.97	2.40	3.336(2)	161.8

Symmetry codes : (i) x, y−1, z; (ii) x, y+1, z; (IV) x+1/2, y−1/2, z; (iv) −x+2, y, −z+1/2; (v) x+1/2, y+1/2, z; (vi) −x+2, y−1, −z+1/2.

Table 3: Frontier molecular orbital calculation for the 1EPBH compound

Quantum Parameters		**E_{HOMO} (eV)**	**E_{LUMO} (eV)**	**$\lvert \Delta E \rvert$ (eV)**	**I**	**A**	**χ**	**η**	**μ**	**ω**	**S**
DFT/ B3LYP/	Gas	-6.77	-1.98	4.79	6.77	1.98	4.78	2.40	-4.78	4.76	0.21

6-311++G(d, p)	Water	-7.18	-1.50	5.68	7.18	1.50	4.34	2.84	-4.34	3.32	0.18
	DMSO	-7.18	-1.49	5.69	7.18	1.49	4.33	2.85	-4.33	3.29	0.18

$\Delta E = |E_{HOMO} - E_{LUMO}|$ (eV), $I = -E_{HOMO}$ (eV), $A = -E_{LUMO}$, $\chi = (I+A)/2$, $\eta = (I-A)/2$, $\mu = -(I+A)/2$, $\omega = \mu^2/2\eta$, $S = 1/2\eta$.

Table 4: Topological parameters of the $(C_6H_{16}N_2)(HC_2O_4)_2$ molecule

Interaction	**$\nabla^2\rho(r)$ (u. a)**	**$\rho(r)$ (u. a)**	**G(r) (u. a)**	**V(r) (u. a)**	**H(r) (u. a)**	**ε**	**$E_{interaction}$ (kJ/mol)**
C_4-H_5...O_{27}	0.0354	0.0119	0.0079	-0.0069	0.0010	0.0970	-9.06
N_{16}-H_{17}...O_{25}	0.1197	0.0992	0.0713	-0.1127	-0.0414	0.0218	-147.95
C_{21}-H_{24}...O_{25}	0.0277	0.0077	0.0039	-0.0049	0.0010	0.5008	-6.43
C_{10}-H_{12}...O_{27}	0.0376	0.0126	0.0084	-0.0073	0.0011	0.0894	-9.58
O_{37}-H_8... N_7	0.0906	0.0654	0.0420	-0.0614	-0.0194	0.0138	-80.60

Table 5: Theoretical and experimental chemical shifts of carbon atoms in the 1EPBH compound

Carbon atoms	**Theoretical δ (ppm) (B3LYP 6-311G)**	**Experimental δ (ppm)**
C1	13460	135
C2	144.6	145
C3	144.63	144.5

C4	139.74	140
C5	132.89	132
C6	177.32	177
C7	25.45	26
C8	24.94	24.5
C9	14.69	14
C10	9.57	9.5

Table 6: Docking calculations of the 1EPBH compound and 3MDZ, 1JCZ, 5Fl5 and 6H36 proteins

Ligand	Proteins	Binding score (kcal/mol)	RMSD refine	Bonds between atoms of the compounds and residues of the active sites			
				Atoms of ligand	Involved receptor residues	Bond types	Distance (A°)
1EPBH	3MDZ	–3.15	1.86	O32	TYR 9	H-donor	2.74
				O33	LYS 101	H-acceptor	3.07
	1JCZ	–5.36	1.39	C11	CYS 232	H-donor	3.62
				O33	TYR 7	H-acceptor	3.04
	5FL5	–3.69	2.01	O36	THR 200	H-acceptor	3.01
	6H36	–3.92	1.40	O31	THR 199	H-donor	3.08
				O36	THR 99	H-acceptor	2.90
				C1	5-RING HIS 94	H-pi	4.35

Declaration of interests

The authors declare that they have no known competing financial interests or personal relationships that could have appeared to influence the work reported in this paper.